AD-A127 246 NEAR FIELD ANALYSIS OF AIRBORNE ANTENNA(U) OHIO STATE UNIV COLUMBUS ELECTROSCIENCE LAB N WANG ET AL. MAR 83 ESL-714215-4 N00019-81-C-0424 1/1

UNCLASSIFIED F/G 9/5 NL

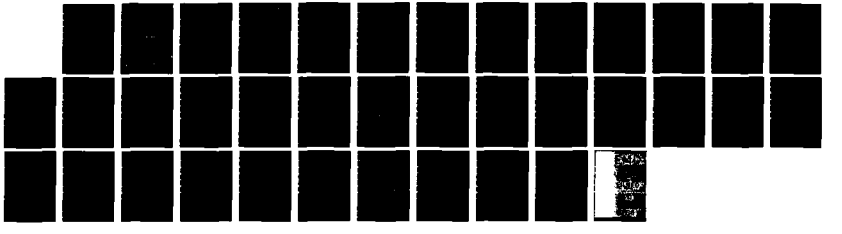

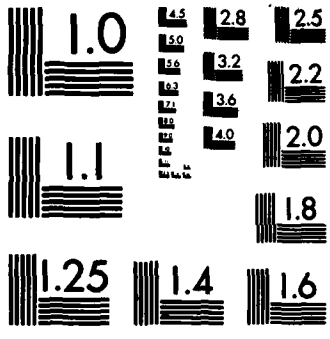

MICROCOPY RESOLUTION TEST CHART
NATIONAL BUREAU OF STANDARDS-1963-A

OSU

The Ohio State University

NEAR FIELD ANALYSIS OF AIRBORNE ANTENNA

Nan Wang and W.D. Burnside

The Ohio State University

ElectroScience Laboratory

Department of Electrical Engineering
Columbus, Ohio 43212

Final Report 714215-4

Contract No. N00019-81-C-0424

March 1983

DTIC
APR 7 1983

Department of the Navy (Code AIR 21512X)
Naval Air Systems Command
Washington, D.C. 20361

APPROVED FOR PUBLIC RELEASE
DISTRIBUTION UNLIMITED

DTIC FILE COPY

83 04 26 099

NOTICES

When Government drawings, specifications, or other data are used for any purpose other than in connection with a definitely related Government procurement operation, the United States Government thereby incurs no responsibility nor any obligation whatsoever, and the fact that the Government may have formulated, furnished, or in any way supplied the said drawings, specifications, or other data, is not to be regarded by implication or otherwise as in any manner licensing the holder or any other person or corporation, or conveying any rights or permission to manufacture, use, or sell any patented invention that may in any way be related thereto.

50272-101

REPORT DOCUMENTATION PAGE	1. REPORT NO.	2.	3. Recipient's Accession No. AD-A127246

4. Title and Subtitle

NEAR FIELD ANALYSIS OF AIRBORNE ANTENNAS

5. Report Date

March 1983

6.

7. Author(s)

Nan Wang and W.D. Burnside

8. Performing Organization Rept. No.

ESL 714215-4

9. Performing Organization Name and Address

The Ohio State University ElectroScience Laboratory
Department of Electrical Engineering
Columbus, Ohio 43212

10. Project/Task/Work Unit No.

11. Contract(C) or Grant(G) No

(C)

(G) N00019-81-C-0424

12. Sponsoring Organization Name and Address

Department of the Navy (Code AIR 21512X)
Naval Air Systems Command
Washington, D.C. 20361

13. Type of Report & Period Covered

Final Report

14.

15. Supplementary Notes

16. Abstract (Limit: 200 words)

The radiation pattern analysis for the ellipsoid based on the efficient UTD and geodesic solution has been completed. This new ellipsoid configuration will be used to represent the fuselage in future aircraft simulation analyses.

17. Document Analysis a. Descriptors

b. Identifiers/Open-Ended Terms

c. COSATI Field/Group

18. Availability Statement

APPROVED FOR PUBLIC RELEASE:
DISTRIBUTION UNLIMITED

19. Security Class (This Report) Unclassified

20. Security Class (This Page) Unclassified

21. No of Pages 30

22. Price

(See ANSI-Z39.18) See Instructions on Reverse

OPTIONAL FORM 272 (4-
(Formerly NTIS-35)
Department of Commerce

TABLE OF CONTENTS

	Page
LIST OF FIGURES	iii
NEAR FIELD ANALYSIS OF AIRBORNE ANTENNAS	1
REFERFENCES	29

Accession For
NTIS GRA&I
DTIC TAB
Unannounced
Justification
By
Distribution/
Availability Codes
Dist Special
A

DTIC COPY INSPECTED 2

LIST OF FIGURES

Figure		Page
1	Roll plane (θ_C=0°, ϕ_C=0°, θ=90°) patterns for a 0.25" monopole mounted at θ_S=90° on a 2λ x 4λ spheroid.	4
2	Roll plane (θ_C=0°, ϕ_C=0°, θ=90°) patterns for a 0.25" monopole mounted at θ_S=90° on a 2λ x 4λ spheroid.	5
3	Various terms used in cylinder/plate model.	6
4	Calculated radiation patterns (θ_C=0°, ϕ_C=0°, θ=90°) for a 0.25" monopole mounted at θ=90°.	7
5	Geodesic paths defined by the surface parameters (θ_Q, ϕ_Q) for a source mounted at θ_S=90° on a 4λ x 6λ x 40λ ellipsoid.	11
6	Geodesic tangents defined by the radial vector direction (θ_t, ϕ_t) for a source mounted at θ_S=90° on a 4λ x 6λ x 40λ ellipsoid.	12
7	Geodesic paths defined by the surface parameters (θ_Q, ϕ_Q) for a source mounted at θ_S=30° on a 4λ x 6λ x 40λ ellipsoid.	13
8	Geodesic tangents defined by the radial vector direction (θ_t, ϕ_t) for a source mounted at θ_S=30° on a 4λ x 6λ x 40λ ellipsoid.	14
9	Geodesic paths defined by the surface parameters (θ_Q, ϕ_Q) for a source mounted at (θ_S=30°, ϕ_S=45°) on a 4λ x 6λ x 40λ ellipsoid.	15
10	Geodesic paths defined by the surface parameters (θ_Q, ϕ_Q) for a source mounted at (θ_S=30°, ϕ_S=70°) on a 4λ x 6λ x 40λ ellipsoid.	16
11	Geodesic tangents defined by the radial vector direction (θ_t, ϕ_t) for a source mounted at (θ_S=30°, ϕ_S=45°) on a 4λ x 6λ x 40λ ellipsoid.	17

Figure		Page
12	Geodesic tangents defined by the radial vector direction (θ_t, ϕ_t) for a source mounted at (θ_S=30°, ϕ_S=70°) on a 4λ x 6λ x 40λ ellipsoid.	18
13a	Comparison of radiation patterns in azimuth plane for a short monopole mounted at ϕ_S=0°, Z_S=-10 on a 4λ x 40λ spheroid.	19
13b	Comparison of radiation patterns in elevation plane for a short monopole mounted at ϕ_S=0°, Z_S=-10 on a 4λ x 40λ spheroid.	20
13c	Comparison of radiation patterns in roll plane for a short monopole mounted at ϕ_S=0°, Z_S=-10 on a 4λ x 40λ spheroid.	21
14a	Comparison of radiation patterns in azimuth plane for a short monopole mounted at ϕ_S=30°, Z_S=-10 on a 4λ x 40λ spheroid.	22
14b	Comparison of radiation patterns in elevation plane for a short monopole mounted at ϕ_S=30°, Z_S=-10 on a 4λ x 40λ spheroid.	23
14c	Comparison of radiation patterns in roll plane for a short monopole mounted at ϕ_S=30°, Z_S=-10 on a 4λ x 40λ spheroid.	24
15a	Radiation patterns in azimuth plane for short monopole mounted at ϕ_S=0°, Z_S=-10 on a 4λ x 8λ x 40λ ellipsoid.	25
15b	Radiation patterns in elevation plane for a short monopole mounted at ϕ_S=0°, Z_S=-10 on a 4λ x 8λ x 40λ ellipsoid.	26
15c	Radiation patterns in roll plane for a short monopole mounted at ϕ_S=0°, Z_S=-10 on a 4λ x 8λ x 40λ ellipsoid.	27

As with most sophisticated systems the demands placed upon them continually increase. This certainly is the case for modern radiating systems where there seem to be ever increasing demands placed on the functions performed, the pattern requirements desired, as well as the wide bandwidth expected. In this report, the question of improved pattern performance is addressed. In order to approach the desired pattern requirements of an airborne antenna system, the antenna designer has been forced to take numerous far field measurements mainly using a scale model of the given aircraft. This approach has not been satisfactory in that it is both expensive and time consuming. That is to say, if the true far field patterns are desired, one must maintain and run continuously a very large antenna range (i.e., the far field of a typical scale model antenna measurements might be in excess of a thousand feet).

As a result of this situation, there has been a great deal of interest in determining the far field patterns based on near field pattern measurements. This so[illegible] very attractive to the antenna designer in that near field measurements can be taken in small anechoic chambers at a greatly reduced cost. In order to determine the far field patterns based on these near field measurements, most of the attention has focused on plane, cylindrical, and spherical wave spectrum approaches. These solutions offer some improvement; however, the transform from the near field to the far field is basically an integral relationship which in itself can be tedious and expensive. The real solution to this problem lies in the fact that one must find a direct

approach that simply converts near field data to the desired far field results. Thus, the following dilemma prevails: far field patterns are desired but it is inefficient to measure them directly; near field patterns are much easier to measure but inefficient to transform to the far field.

The concept applied here is to use a new theoretical approach to this problem which is valid in both the near and far field such that it can be verified by a near field measurement. Once this is accomplished, it can be used directly to compute the far field pattern. Using this concept, one can very efficiently examine various antenna designs based on far field pattern requirements. As interesting configurations evolve, one can take various near field measured patterns to verify the theoretical solution. Furthermore, these near field patterns might even be measured on the actual aircraft sitting on the flight line. The basic philosophy here is that one can use the numerical solution to predict the pattern performance for a given application such that one can easily narrow the alternatives down to a few practical solutions. At this point, some type of measurement, either near or far field pattern, could be made using either a scale model or the actual aircraft in order to verify the numerical result. Using this approach one can quickly examine various possibilities and determine an optimum solution.

The first major numerical solution for airborne antenna patterns concentrated on using a cylindrical fuselage as described in References [1,2,3]. The limitation of the analysis to a cylindrical fuselage

resulted for two major reasons: 1) the geodesics on a general curved surface are not straightforward, and 2) the radiation pattern solution for antennas mounted on a general curved surface with torsion was not available. Both of these obstacles have been overcome under the continuating support from the Naval Air System Command (NASA) contracts as summarized in Reference [4].

The geodesics for complex shapes now can be efficiently determined as shown in Reference [5]. Only flat plate structures need to be added to that solution. Note that it has been shown in References [1,2,3] that one can successfully model complex aircraft structures using finite flat plates.

A prolate spheriod was initially chosen to simulate the fuselage for this study, in that its performance is much easier to evaluate based on comparisons with experimental results. The addition of an isolated flat plate to the prolate spheriod-mounted antenna model was treated in Reference [6]. Some examples of that study are illustrated in Figures 1 and 2. Note that in each case the computed patterns agree very well with the experimental results. The various mechanisms used in that analysis are illustrated in Figure 3 with the individual pattern contributions show in Figure 4. The patterns are all normalized to the same total pattern maximum so that one can get a feel for the significance of the various terms.

The isolated plate study just described follows standard high frequency techniques such that one might anticipate the previous verification for the solution; however, the attachment of the flat

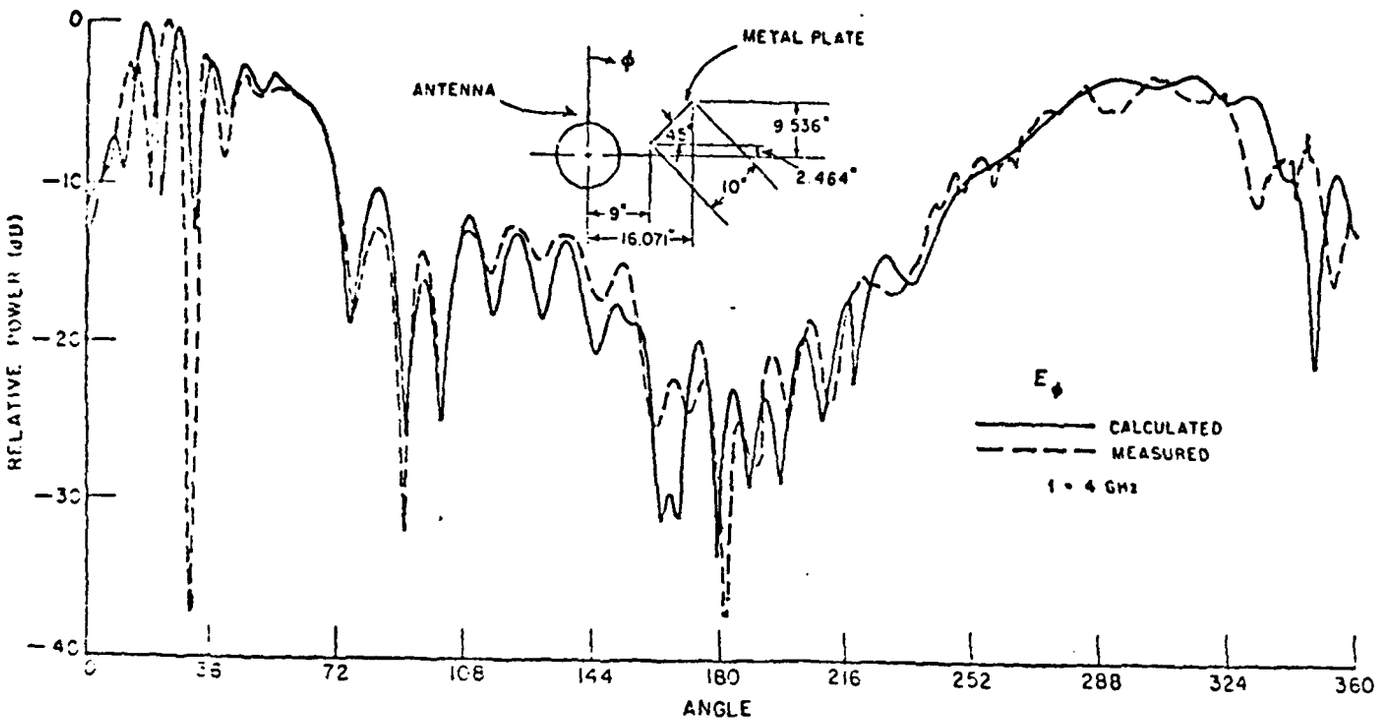

Figure 1. Roll plane (θ_C=0°, ϕ_C=0°, θ=90°) patterns for a 0.25" monopole mounted at θ_S=90° on a 2λ x 4λ spheroid.

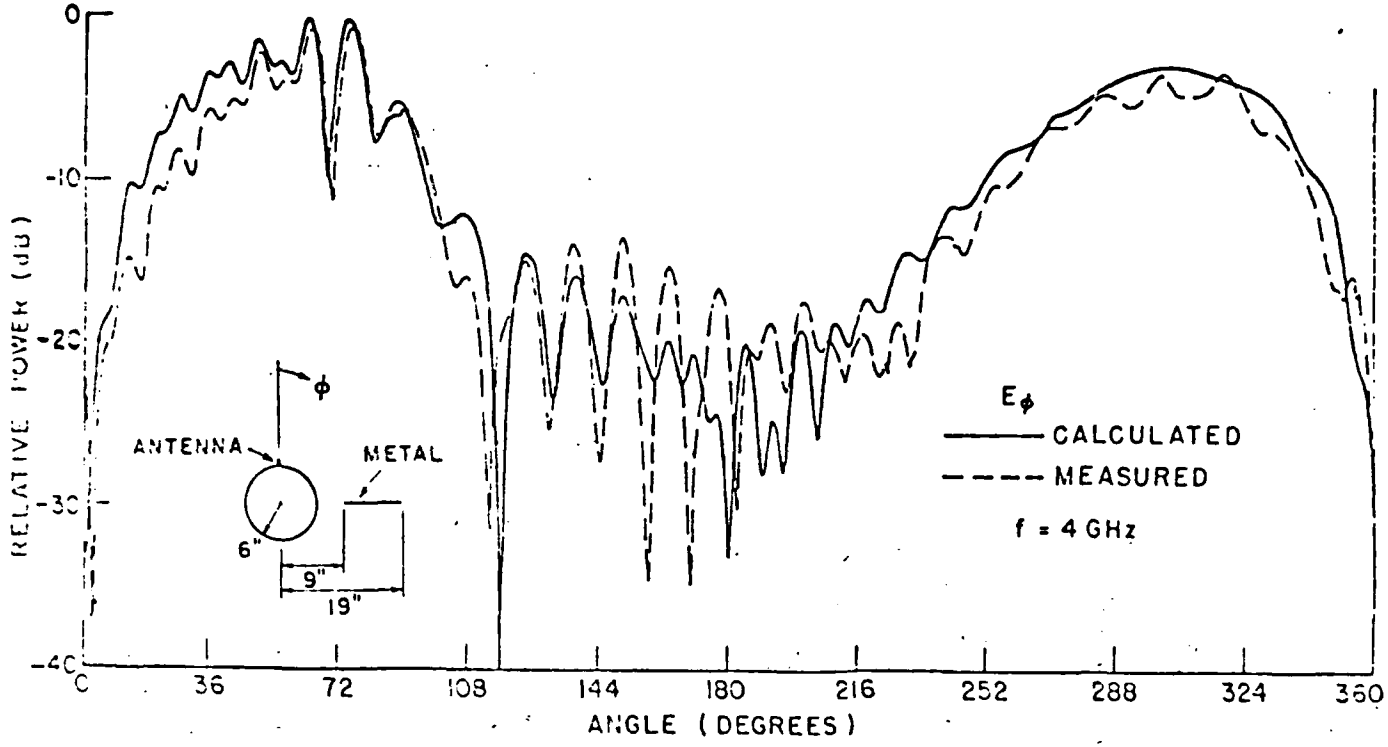

Figure 2. Roll plane ($\theta_c=0°$, $\phi_c=0°$, $\theta=90°$) patterns for [illegible]ole mounted at $\theta_s=90°$ on a $2\lambda \times 4\lambda$ spheroid.

SOLUTION IS OBTAINED BY SUPERPOSITION
OF THE FOLLOWING FIELDS:

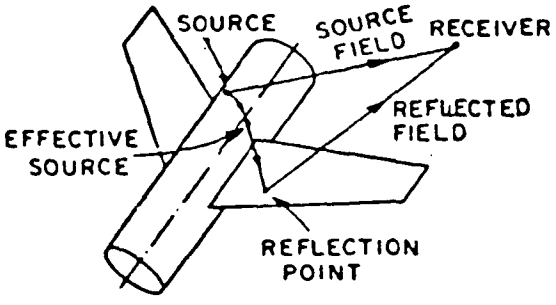

1. DIRECT SOURCE FIELD
2. REFLECTED FIELD

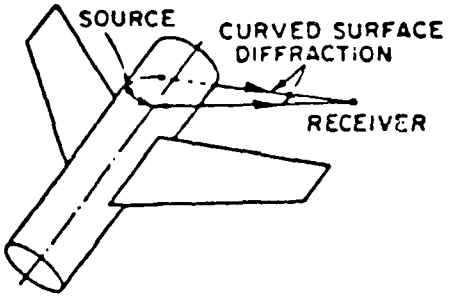

3. CURVED SURFACE DIFFRACTION

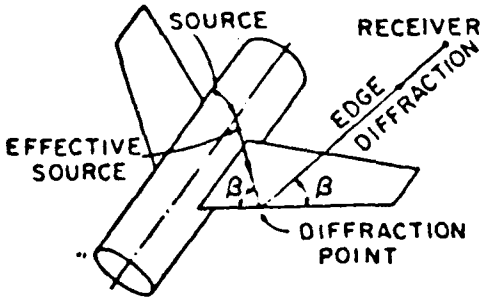

4. EDGE DIFFRACTION

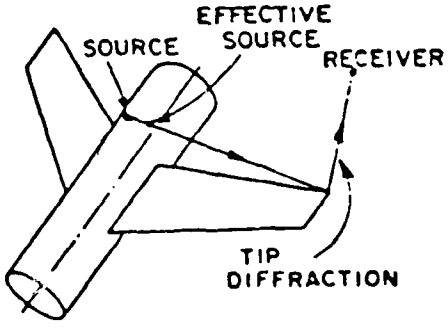

5. TIP DIFFRACTION

Figure 3. Various terms used in cylinder/plate model.

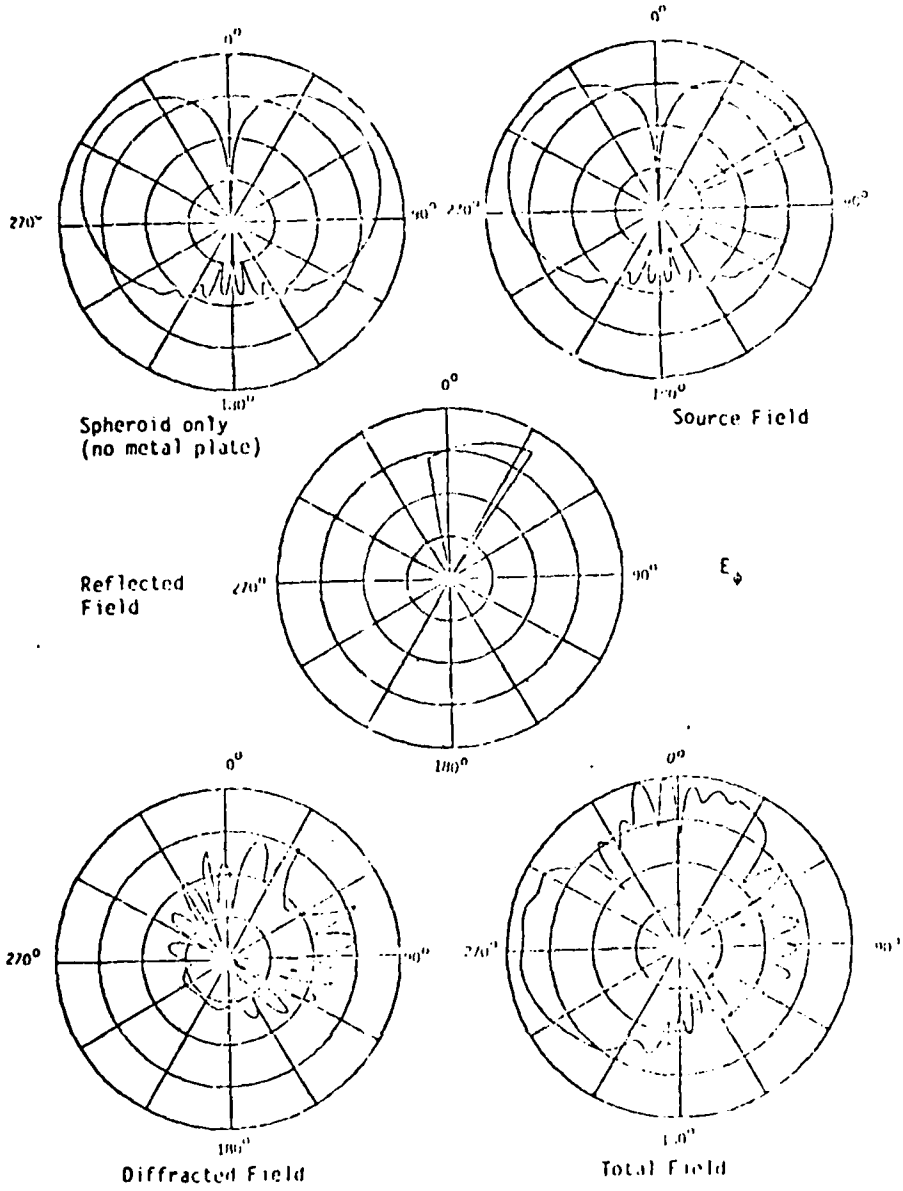

Figure 4. Calculated radiation patterns (θ_c=0°, ϕ_c=0°, θ=90°) for a 0.25" monopole mounted at θ=90°. The metal plate is a 10" x 10" square.

plate to the prolate spheriod is not straightforward. Note that the flat plate must intersect the spheriod in order to represent, for example, the wing-root section of the aircraft.

The study to determine the intersection line between the plate and spheriod was completed using the method described in Reference [7]. The diffractions from this junction line had to be analyzed before a complete radiation pattern could be computed. It was shown in Reference [8] that one could use a modification of the geodesic solution of Reference [5] to determine the illumination of this curved edge. Further, it was found that the radiation solution of Reference [9] could be used to predict the fields incident upon the edges. The edge diffracted fields, then, simply follow the ordinary edge diffraction results of Reference [10].

With the analysis of the junction edge completed and using edge diffraction concepts presented in Reference [3], the complete radiation pattern for an antenna mounted on the aircraft could be computed using the prolate spheroid fuselage simulation. This solution was, then, applied to previous commercial aircraft simulations for which measured results were already available. The significance of this new solution is that the spheroid model provides the proper polarization and curvature effects as opposed to the cylinder which models only one curvature. Note that the surface geometry dictates the polarization of the radiated field [9].

The numerical solution for the analysis of airborne antenna patterns using a prolate spheriod to simulate the fuselage and flat

plates to model the other appendages has been successfully completed. Recall that the flat plate simulations of wings, stabilizers, engines, and stores was very successfully developed and verified under our previous contracts. However, the prolate spheriod representation of the fuselage is not general enough to satisfactorally approximate the wide variety of military aircraft. Note that the prolate spheroid was analyzed initially to illustrate how one can use a simplified geodesic method along with the general GTD radiation solutions to obtain the complete patterns for an antenna mounted on a doubly curved surface. The inadequacy associated with the prolate spheroid model results from its circular cross-section. It has been shown in Reference [1] that an elliptic cross-section is necessary to successfully simulate the wide variety of aircraft fuselage shapes. Since an elliptic cross-section, as well as profile is needed, it is rather obvious that one must use an ellipsoid in order to simulate a general fuselage. Note that the near-zone radiation pattern solution for antennas mounted on a general curved surface with torsion has been developed under the NASC contracts [9]. An essential step in employing the Uniform Geometrical Theory of Diffraction (UTD) to antenna problem is to determine, efficiently, the geodesic paths on the curved surface. In the final year of the NASC contracts (Contract N00019-81-C-0474), an efficient, approximate solution for the geodesic paths on the ellipsoid surface has been obtained [11]. The geodesic paths were tested for various antenna locations on typical ellipsoid surfaces. Another elaborate method for geodesic paths employing the calculus of variations is also presented to show the

validity of the approximated solution. Figures 5-8 are presented in this report to demonstrate the good agreement between the two solutions. The detailed analysis of the geodesic solutions can be found in the quarterly report [11].

Since the ellipsoid is not a surface of revolution, it is necessary to take into account the various antenna locations on the ellipsoid surface. Therefore, the geodesic solution obtained for the top-mounted case [11] was extended to the more general case, i.e., when the antenna is side-mounted on the ellipsoid surface. This new geodesic solution which is valid for an arbitrary antenna location on the ellipsoid surface, is presented in a quarterly report [12]. Some typical results are presented in Figures 9-12. Again, excellent agreement between the rigorous and approximate solutions is obtained.

Now that the geodesic paths on the ellipsoid surface are rounding into shape, the solution is being implemented into the computer code and being applied to obtain radiation patterns for antennas mounted on the ellipsoid surface. To check the validity of this program, the radiation patterns due to an antenna mounted on a spheroid surface are calculated and presented in Figures 13 and 14. It is found that the results compare well with that obtained previously from the spheroid model [6]. Next, the program is being employed to calculate patterns due to antennas mounted on a ellipsoid surface. Typical results are presented in Figure 15. For more numerical results and geometries, one is referred to the quarterly reports [13,14].

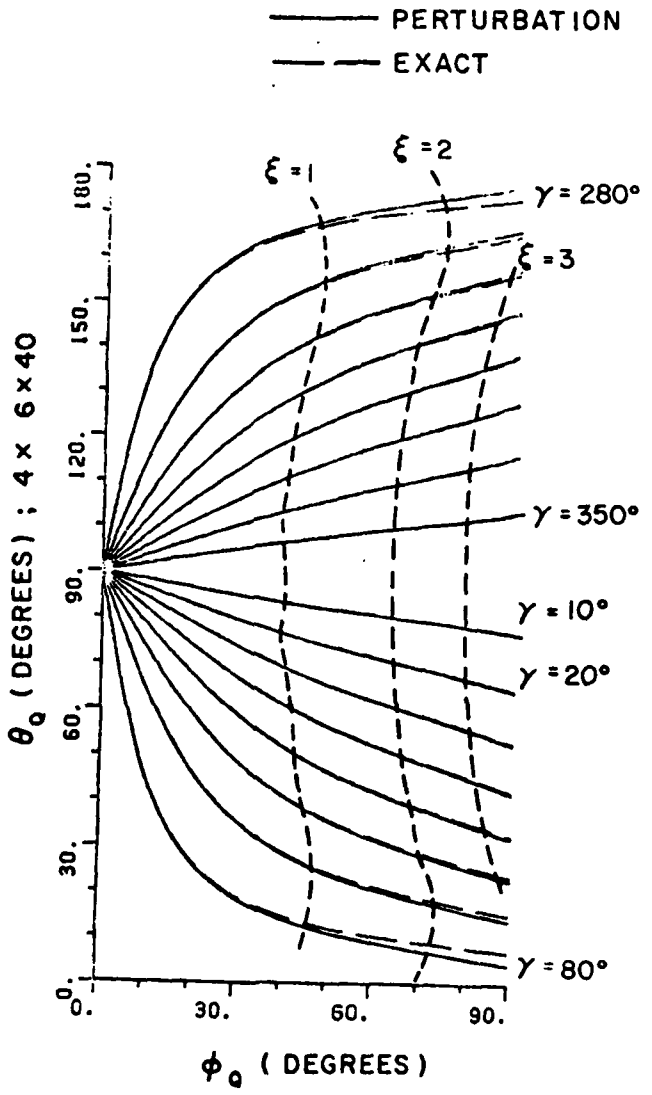

Figure 5. Geodesic paths defined by the surface parameters (θ_0, ϕ_0) for a source mounted at $\theta_s=90^\circ$ on a 4λ x 6λ x 40λ ellipsoid.

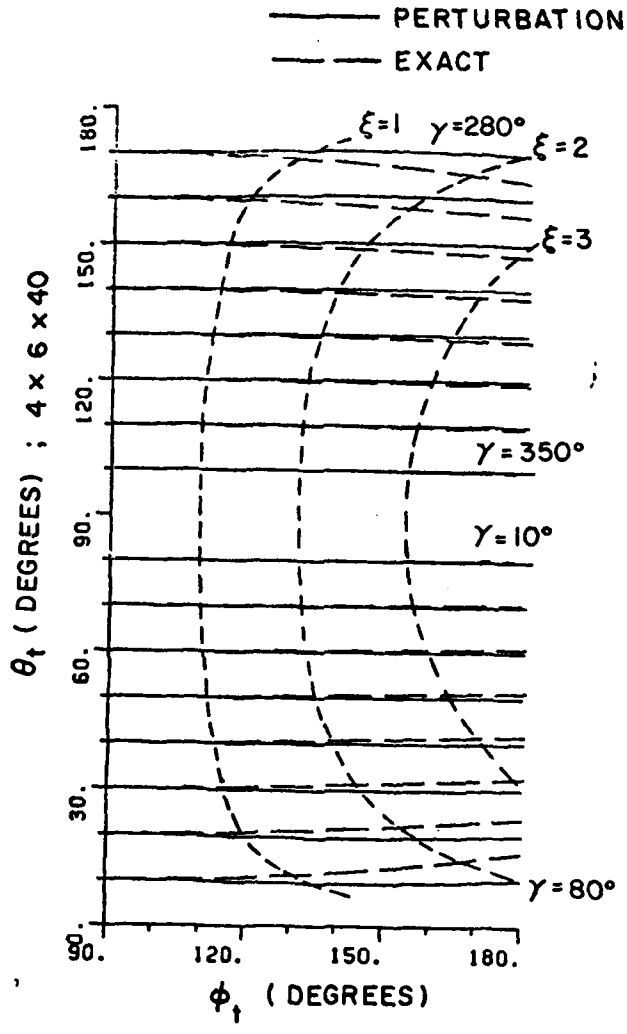

Figure 6. Geodesic tangents defined by the radial vector direction (θ_t, ϕ_t) for a source mounted at $\theta_s=90^\circ$ on a 4λ x 6λ x 40λ ellipsoid.

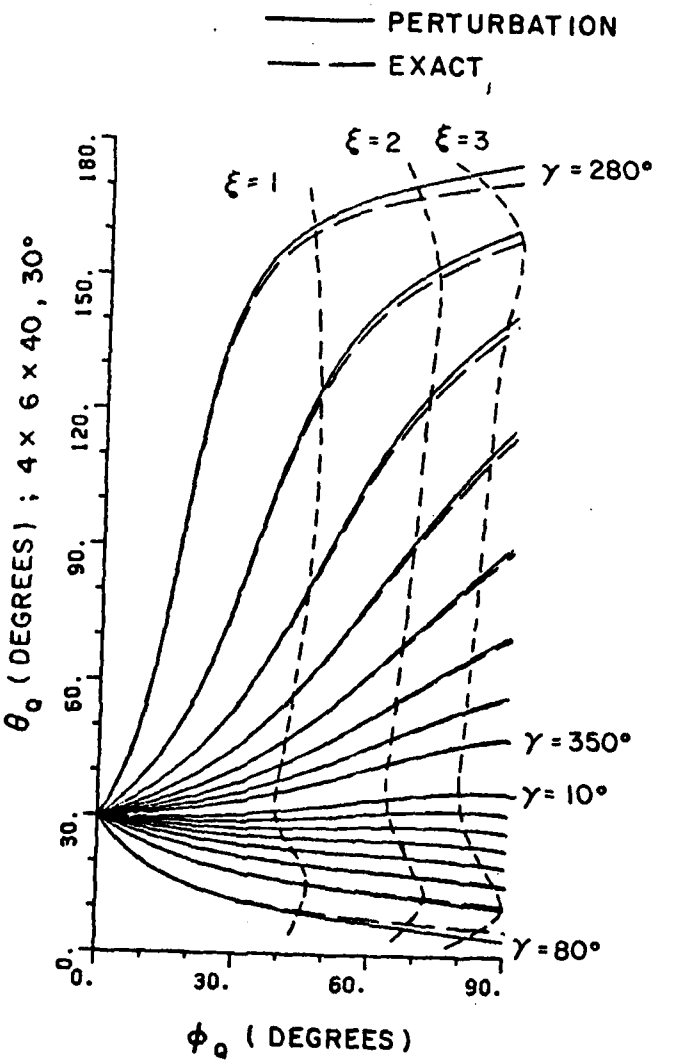

Figure 7. Geodesic paths defined by the surface parameters (θ_0, ϕ_0) for a source mounted at $\theta_s=30^\circ$ on a $4\lambda \times 6\lambda \times 40\lambda$ ellipsoid.

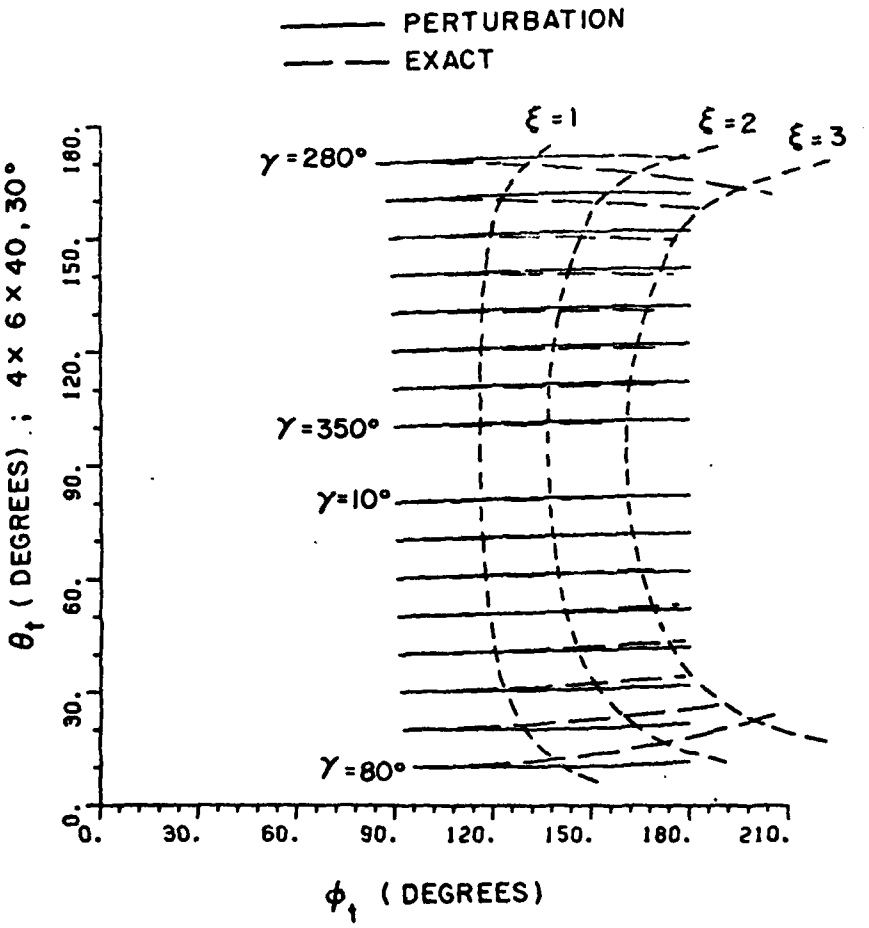

Figure 8. Geodesic tangents defined by the radial vector direction (θ_t, ϕ_t) for a source mounted at $\theta_s = 30°$ on a 4λ x 6λ x 40λ ellipsoid.

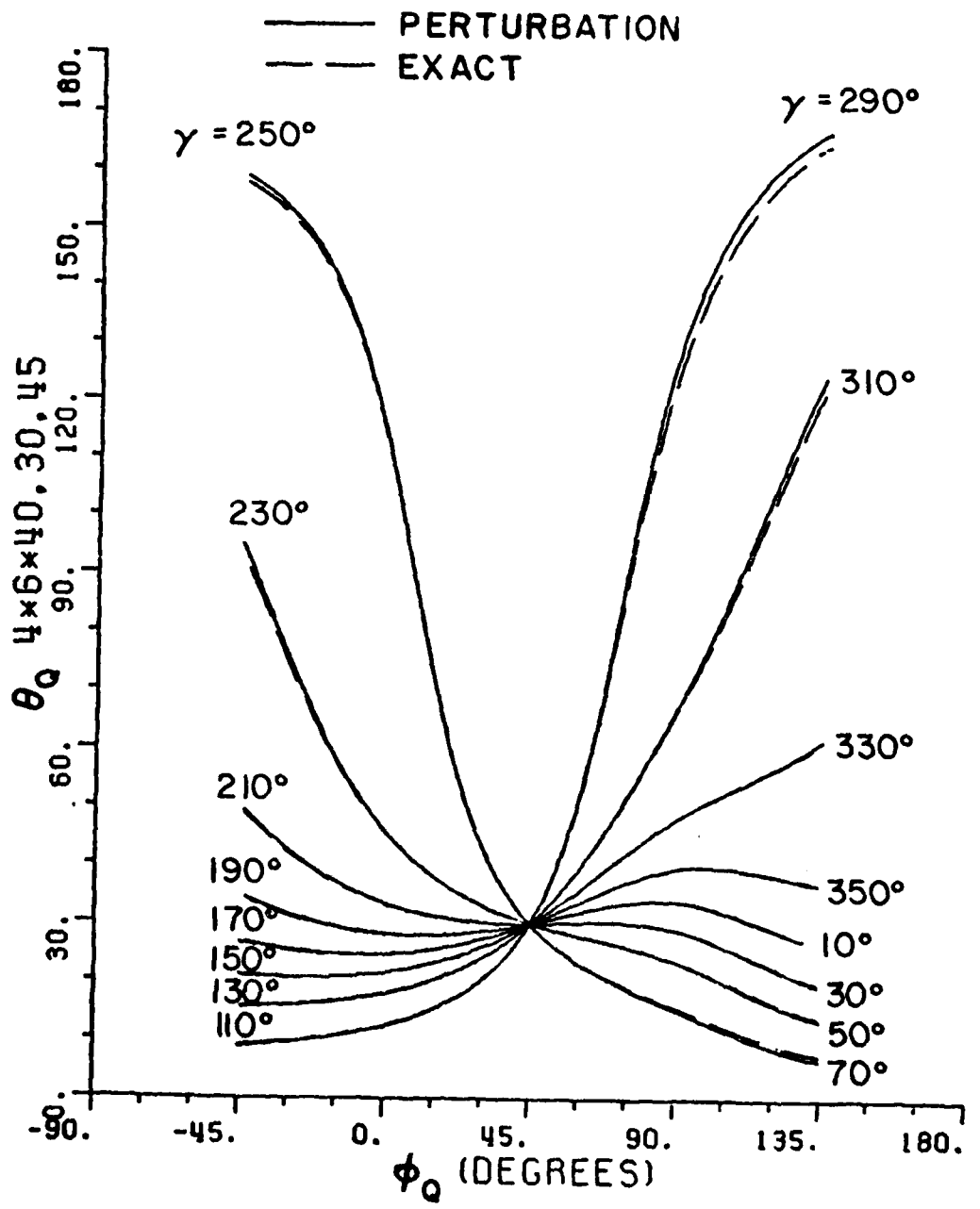

Figure 9. Geodesic paths defined by the surface parameters (θ_Q, ϕ_Q) for a source mounted at $(\theta_S=30^\circ, \phi_S=45^\circ)$ on a $4\lambda \times 6\lambda \times 40\lambda$ ellipsoid.

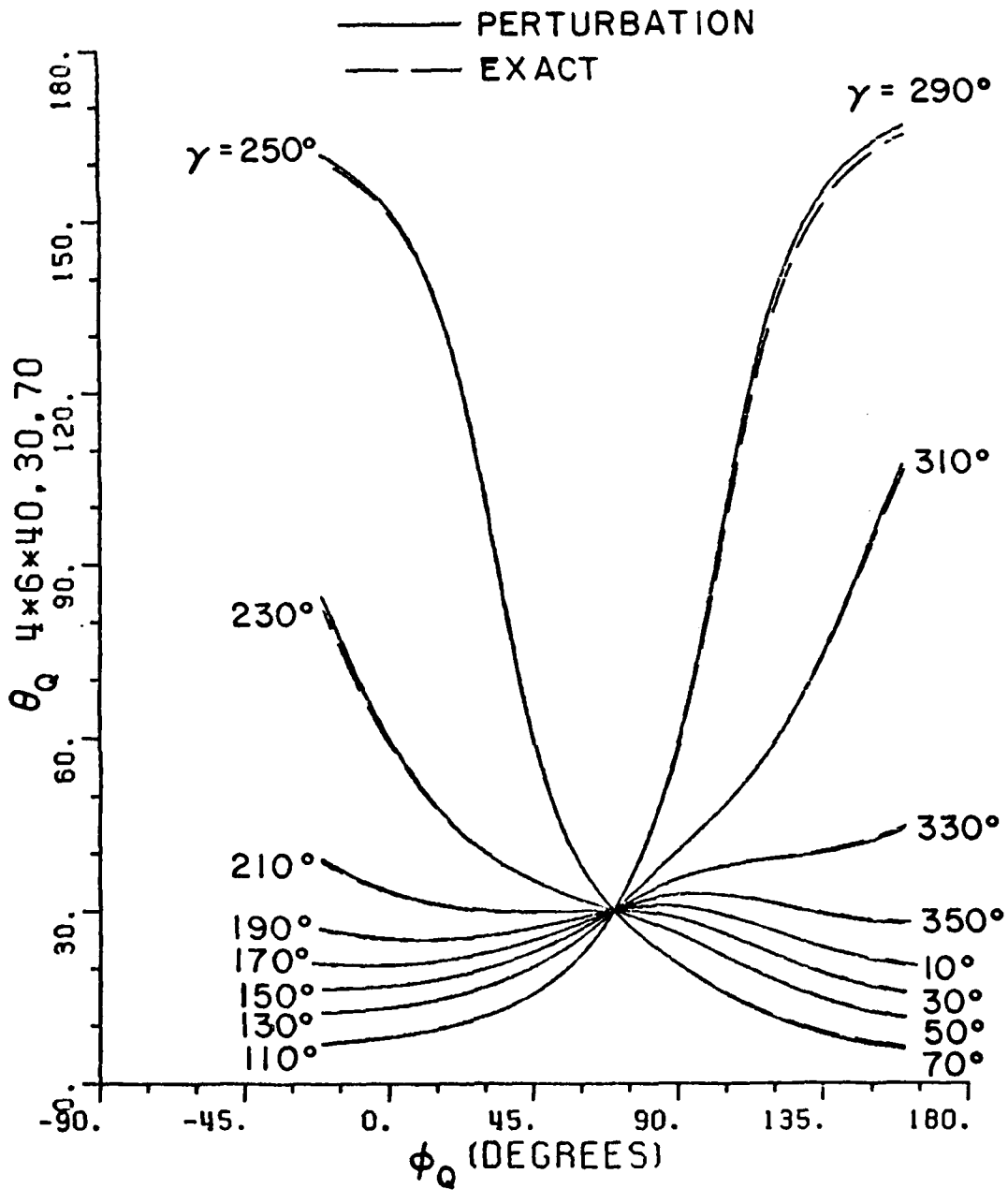

Figure 10. Geodesic paths defined by the surface parameters (θ_Q, ϕ_Q) for a source mounted at $(\theta_S=30^\circ, \phi_S=70^\circ)$ on a $4\lambda \times 6\lambda \times 40\lambda$ ellipsoid.

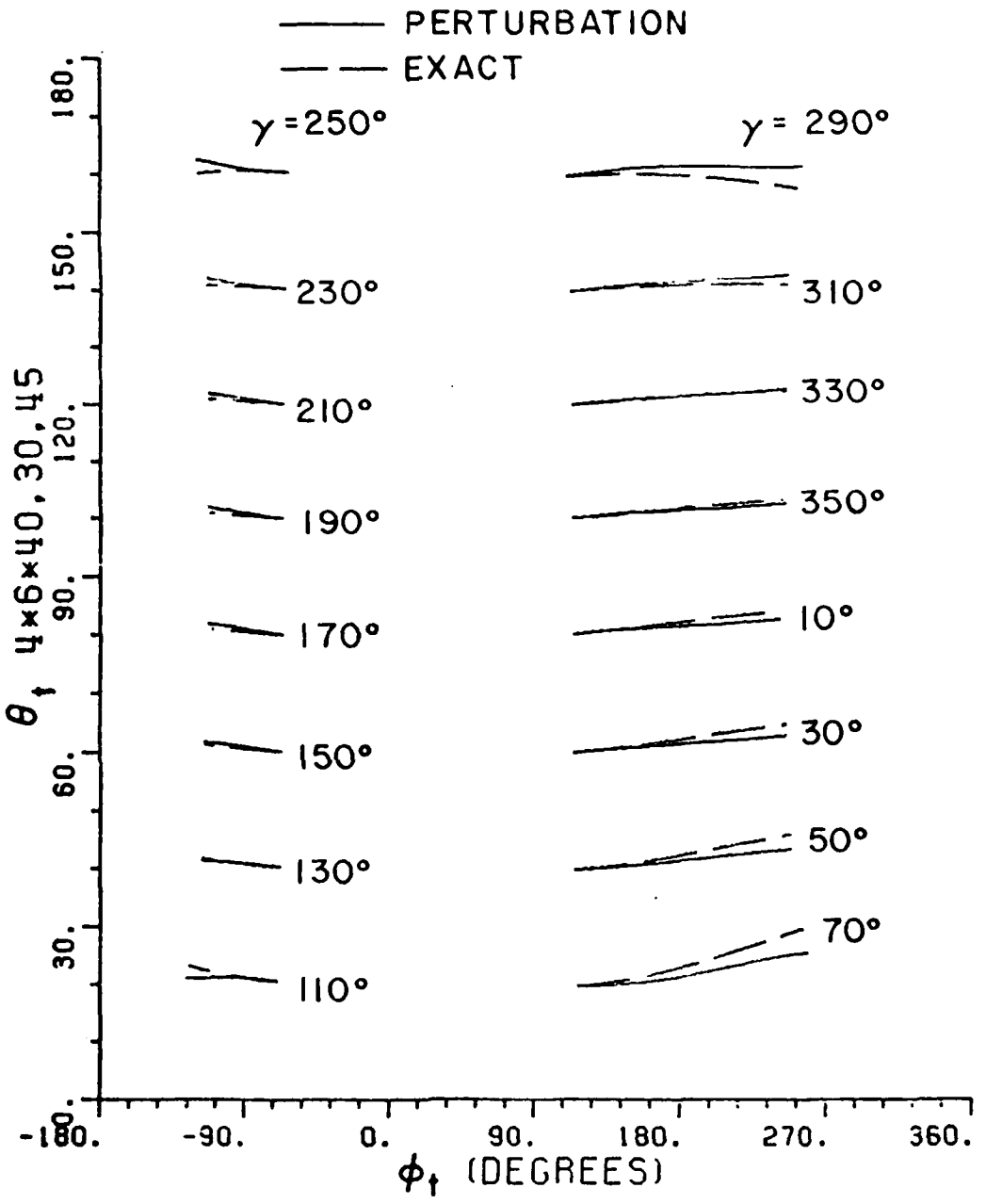

Figure 11. Geodesic tangents defined by the radial vector direction (θ_t, ϕ_t) for a source mounted at (θ_s=30°, ϕ_s=45°) on a 4λ x 6λ x 40λ ellipsoid.

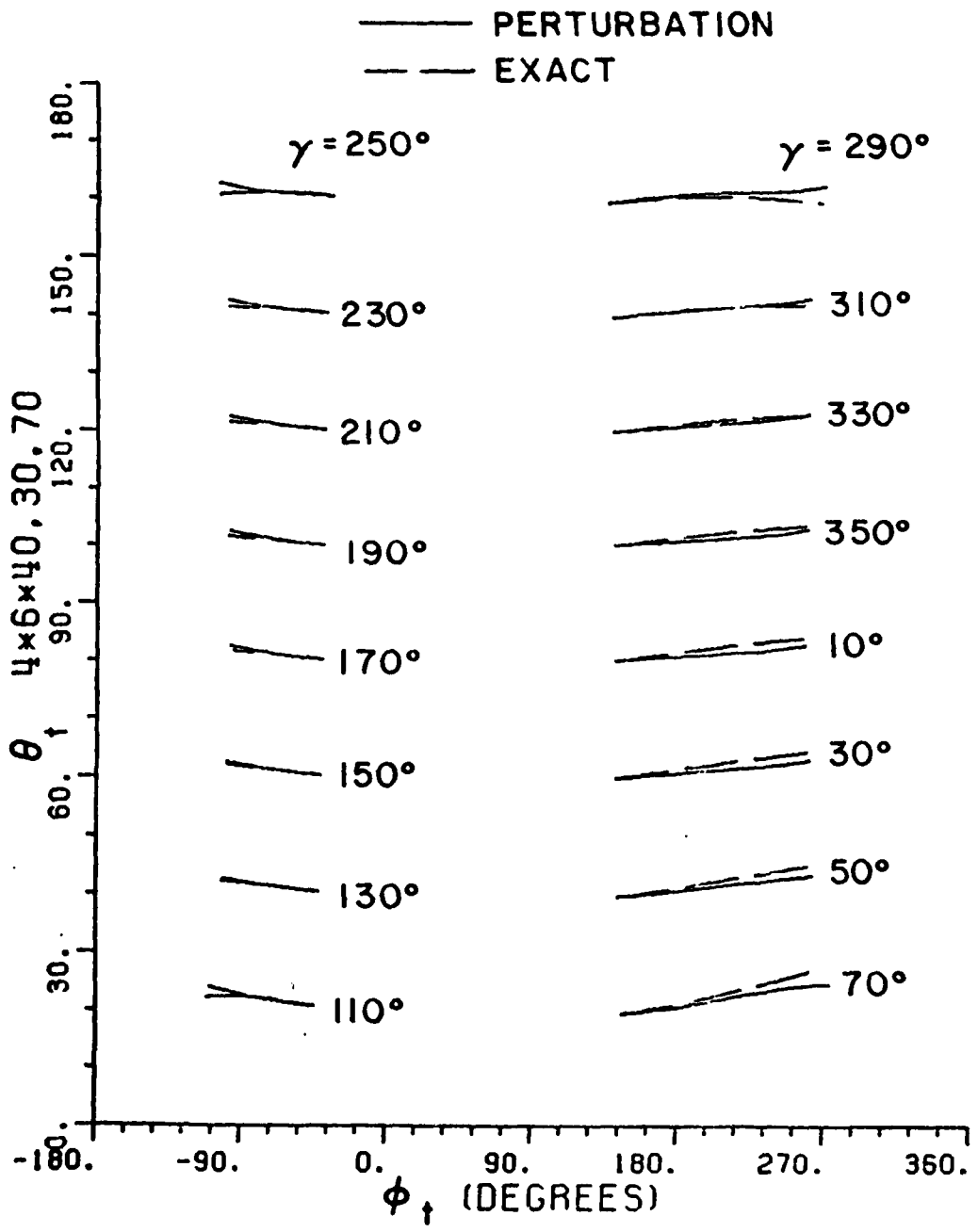

Figure 12. Geodesic tangents defined by the radial vector direction (θ_t, ϕ_t) for a source mounted at $(\theta_s=30^\circ, \phi_s=70^\circ)$ on a $4\lambda \times 6\lambda \times 40\lambda$ ellipsoid.

E_ϕ ——

E_θ - - -

```
UN:METERS
1
FQ:0.3 GHZ
1,0.3,0.3
FG:FUSELAGE
4.,4.,40.
0.,0.,0.
SG:MONOPOLE
0.,-10.
1
0.,0.
.1,.2,0.,.01,3
1.,0.
PD:AZIMUTH PLANE PATTERN (NEAR FIELD)
90.,0.,130.
0,360,1
F,50.
PP:POLAR PLOT IN DB
T
2.,2.5,3
EX:
```

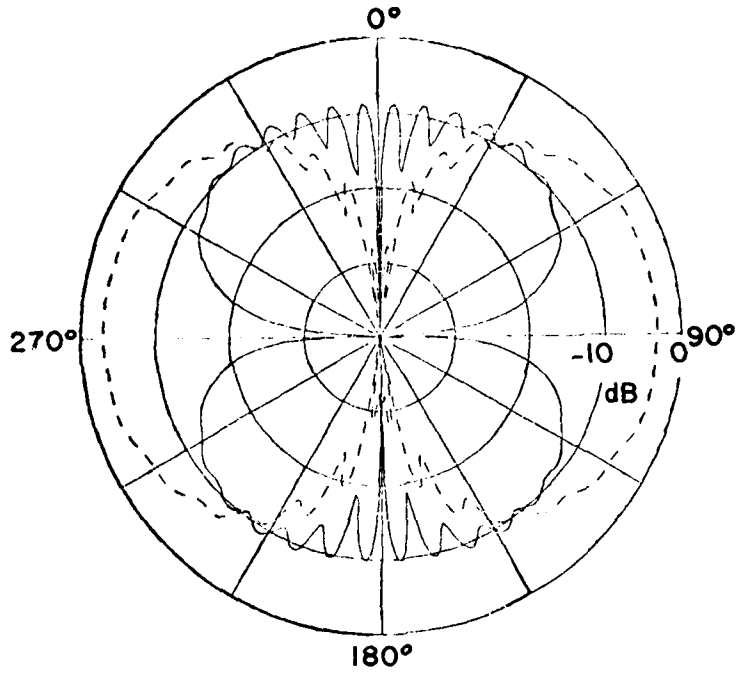

(a) Ellipsoid Program

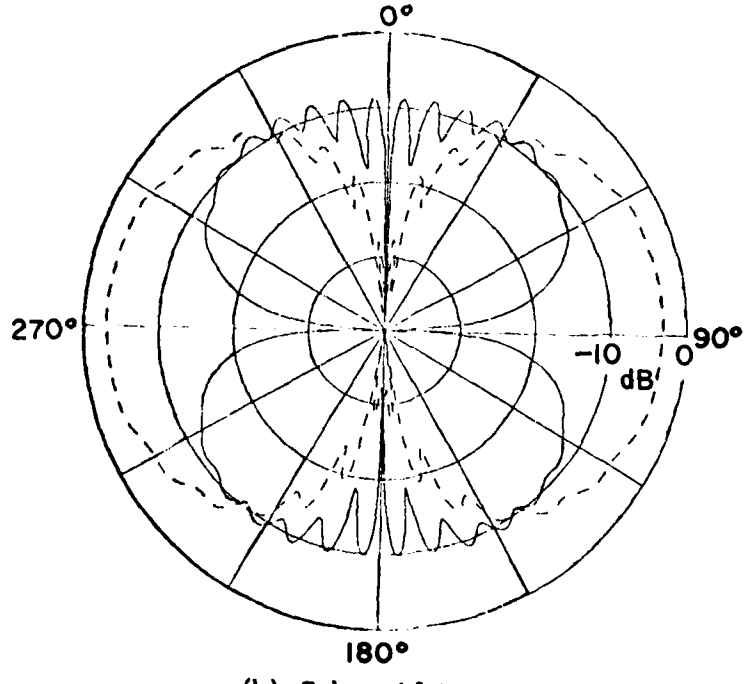

(b) Spheroid Program

Figure 13a. Comparison of radiation patterns in azimuth plane for a short monopole mounted at $\phi_S=0^\circ$, Z_S = -10 on a 4λ x 40λ spheroid.

E_ϕ ——

E_θ - - -

```
UN:METERS
1
FQ:0.3 GHZ
1,0.3,0.3
FG:FUSELAGE
4.,4.,40.
0.,0.,0.
SG:MONOPOLE
0.,-10.
1
0.,0.
.1,.2,0.,.01,3
1.,0.
PD:ELEVATION PLANE PATTERN (FAR FIELD)
90.,90.,130.
0,360,1
T,1000.
PP:POLAR PLOT IN DB
T
2.,2.5,3
EX:
```

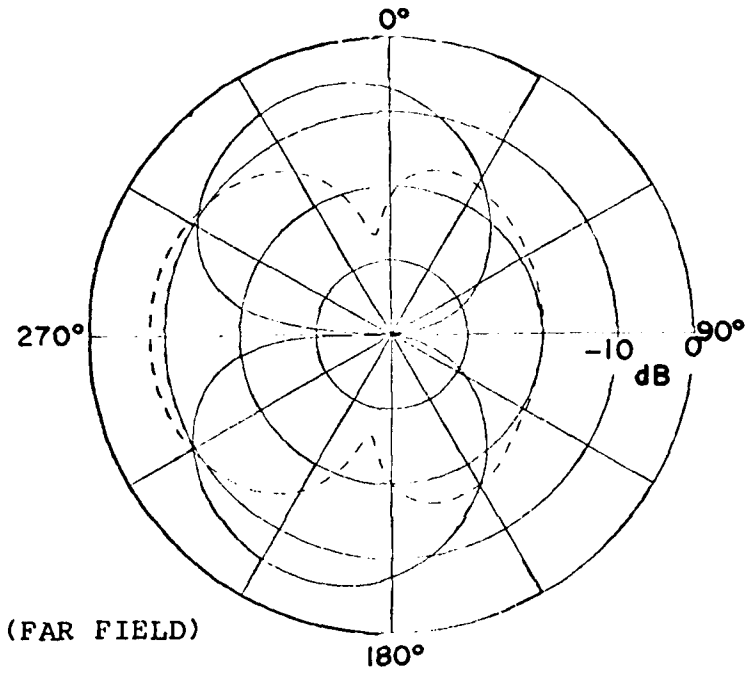

(a) Ellipsoid Program

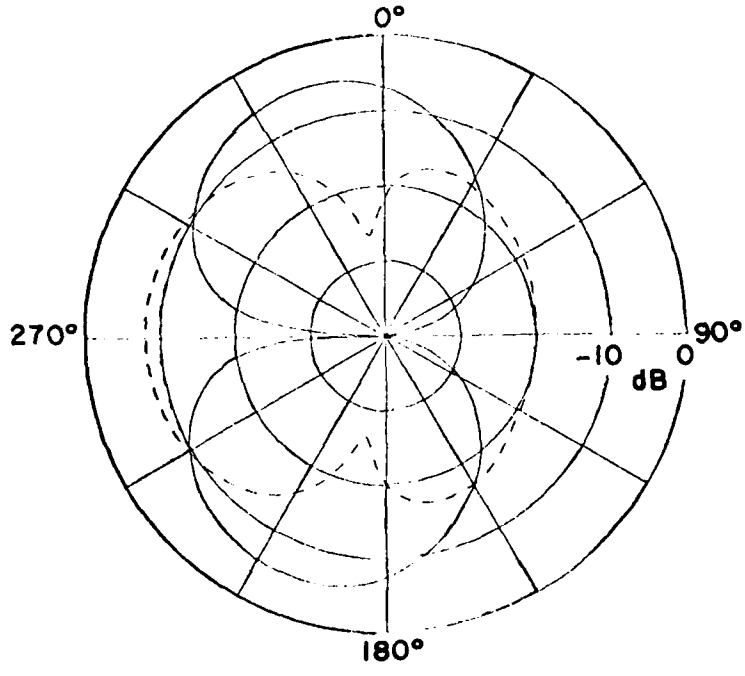

(b) Spheroid Program

Figure 13b. Comparison of radiation patterns in elevation plane for a short monopole mounted at $\phi_S=0^\circ$, Z_S = -10 on a 4λ x 40λ spheroid.

```
UN:METERS
1
FQ:0.3 GHZ
1,0.3,0.3
FG:FUSELAGE
4.,4.,40.
0.,0.,0.
SG:MONOPOLE
0.,-10.
1
0.,0.
.1,.2,0.,.01,3
1.,0.
PD:ROLL PLANE PATTERN (FAR FIELD)
0.,90.,130.
0,360,1
T,1000.
PP:POLAR PLOT IN DB
T
2.,2.5,3
EX:
```

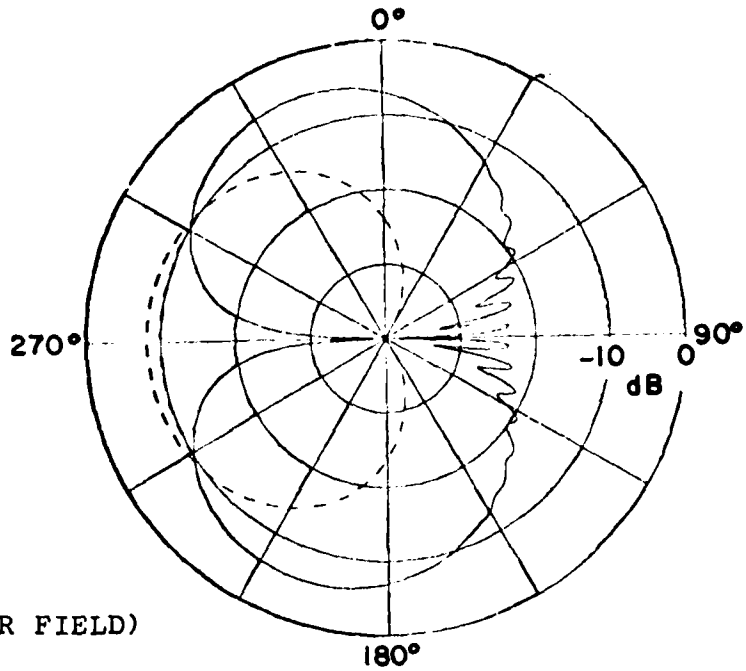

(a) Ellipsoid Program

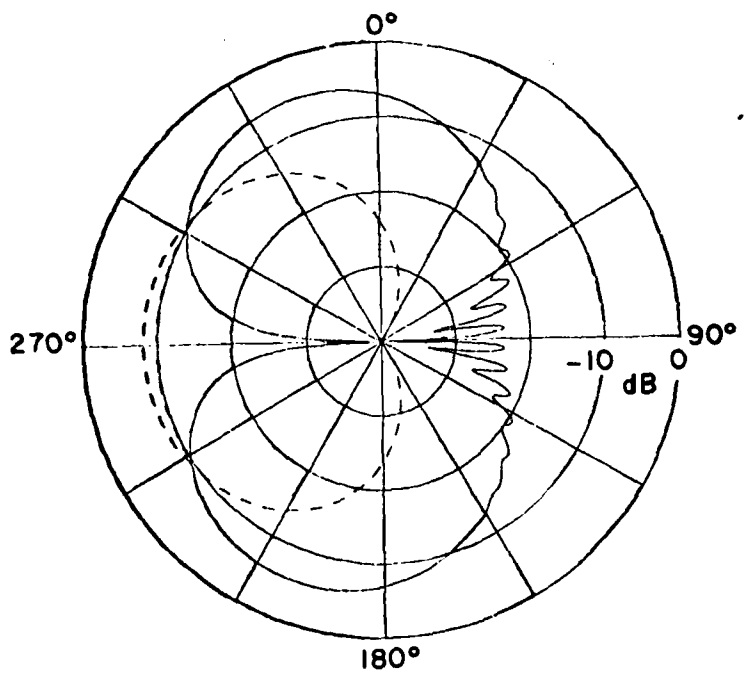

(b) Spheroid Program

Figure 13c. Comparison of radiation patterns in roll plane for a short monopole mounted at $\phi_s=0^\circ$, Zs = -10 on a 4λ x 40λ spheroid.

```
UN:METERS
1
FO:0.3 GHZ
1.0.3.0.3
FG:FUSELAGE
4.,4.,40.
0.,0.,0.
SG:MONOPOLE
30.,-10.
1
0.,0.
.1,.2,0.,.01.3
1.,0.
PD:AZIMUTH PLANE PATTERN (FAR FIELD)
90.,0.,90.
0,360,1
T.1000.
PP:POLAR PLOT IN DB
T
2.,2.5,3
EX:
```

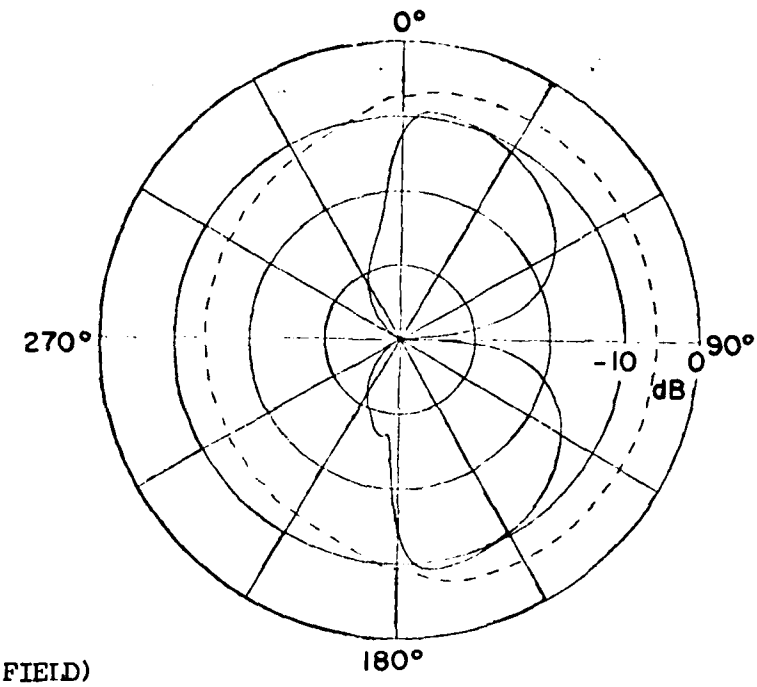

(a) Ellipsoid Program

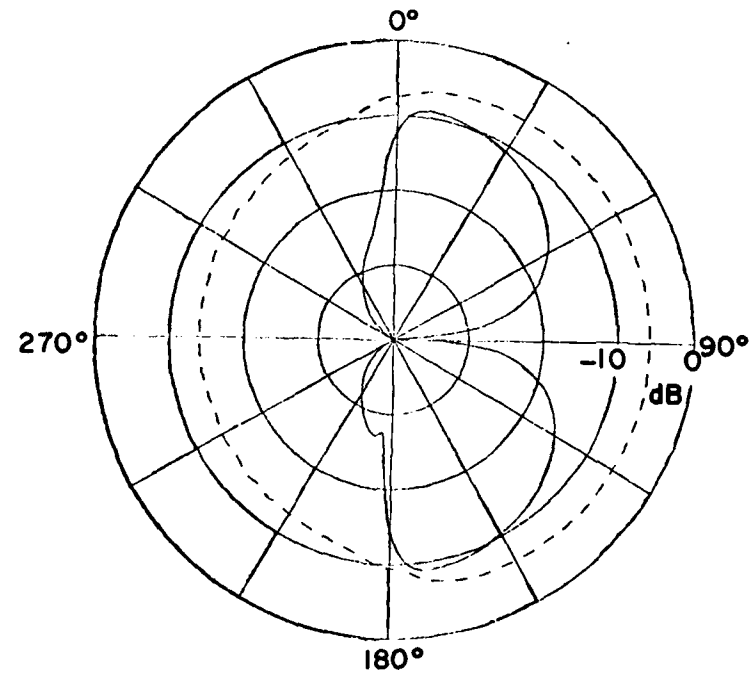

(b) Spheroid Program

Figure 14a. Comparison of radiation patterns in azimuth plane for for a short monopole mounted at ϕ_S=30°, Z_S = -10 on a 4λ x 40λ spheroid.

```
UN:METERS
1
FQ:0.3 GHZ
1,0.3,0.3
FG:FUSELAGE
4.,4.,40.
0.,0.,0.
SG:MONOPOLE
30.,-10.
1
0.,0.
.1,.2,0.,.01,3
1.,0.
PD:ELEVATION PLANE PATTERN (FAR FIELD)
90.,90.,90.
0,360,1
T,1000.
PP:POLAR PLOT IN DB
T
2.,2.5,3
EX:
```

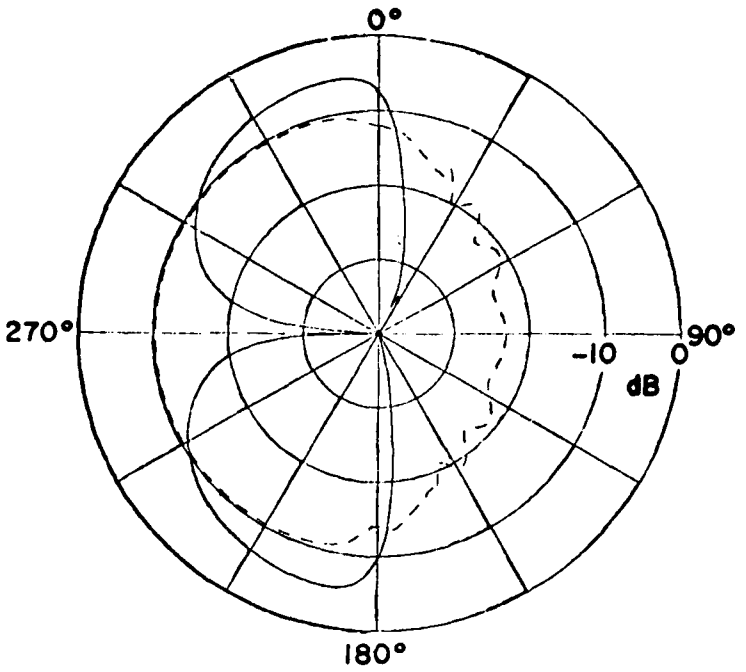

(a) Ellipsoid Program

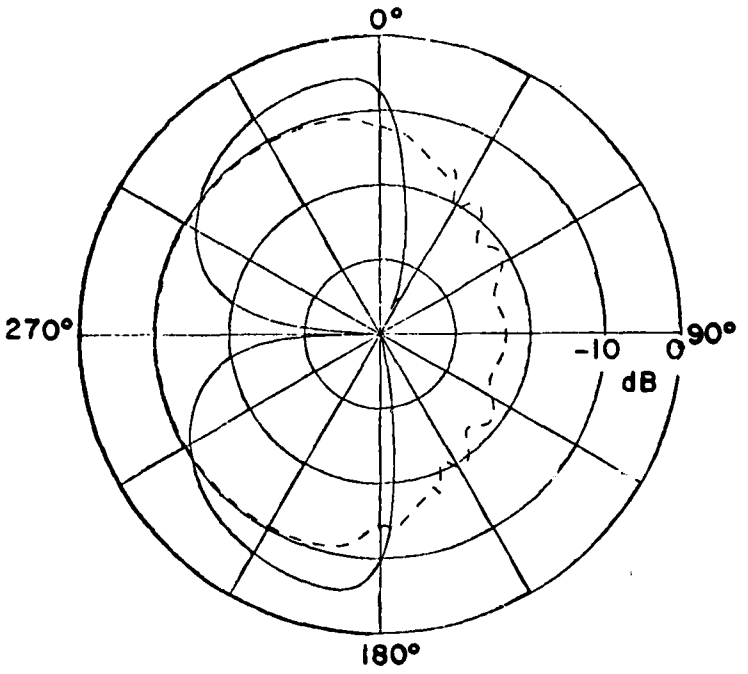

(b) Spheroid Program

Figure 14b. Comparison of radiation patterns in elevation plane for a short monopole mounted at $\phi_s=30^\circ$, Zs = -10 on a 4λ x 40λ spheroid.

```
UN:METERS
1
FO:0.3 GHZ
1,0.3,0.3
FG:FUSELAGE
4.,4.,40.
0.,0.,0.
SG:MONOPOLE
30.,-10.
1
0.,0.
.1,.2,0.,.01,3
1.,0.
PD:ROLL PLANE PATTERN (FAR FIELD)
0.,90.,90.
0,360,1
T,1000.
PP:POLAR PLOT IN DB
T
2.,2.5,3
EX:
```

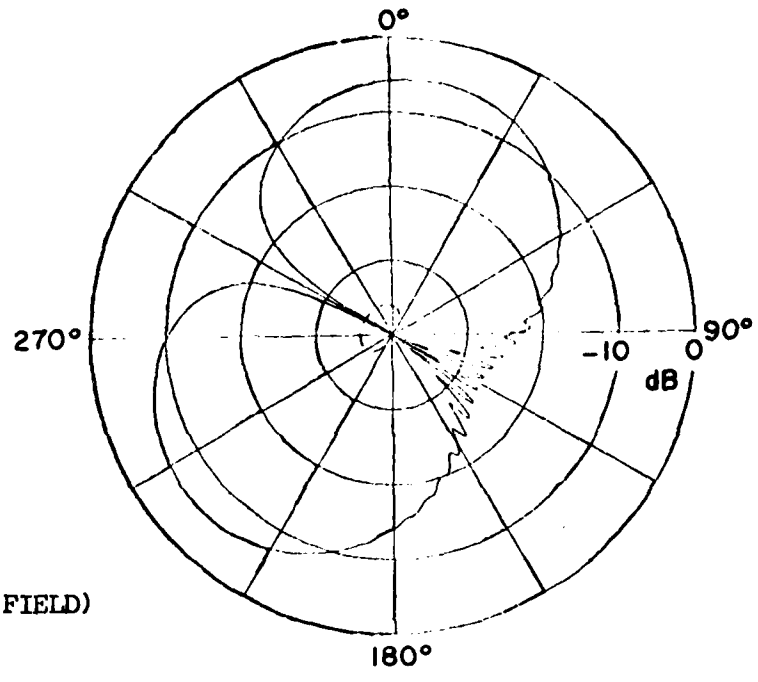

(a) Ellipsoid Program

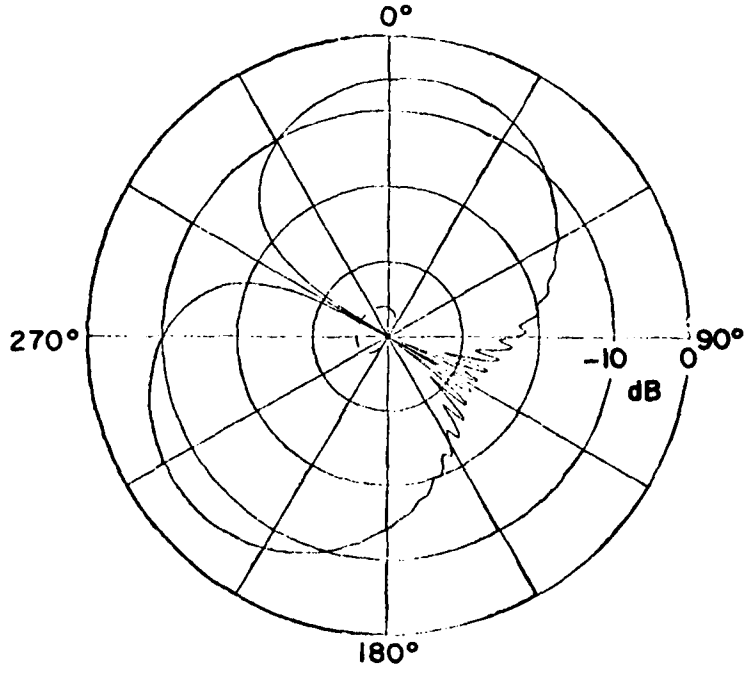

(b) Spheroid Program

Figure 14c. Comparison of radiation patterns in roll plane for a short monopole mounted at $\phi_s=30^\circ$, Zs = -10 on a 4λ x 40λ spheroid.

```
UN:METERS
1
FQ:0.3 GHZ
1,0.3,0.3
FG:FUSELAGE
4.,8.,40.
0.,0.,0.
SG:MONOPOLE
0.,-10.
1
0.,0.
.1,.2,0.,.01,3
1.,0.
PD:AZIMUTH PLANE PATTERN (FAR FIELD)
90.,0.,130.
0,360,1
T,1000.
PP:POLAR PLOT IN DB
T
2.,2.5,3
EX:
```

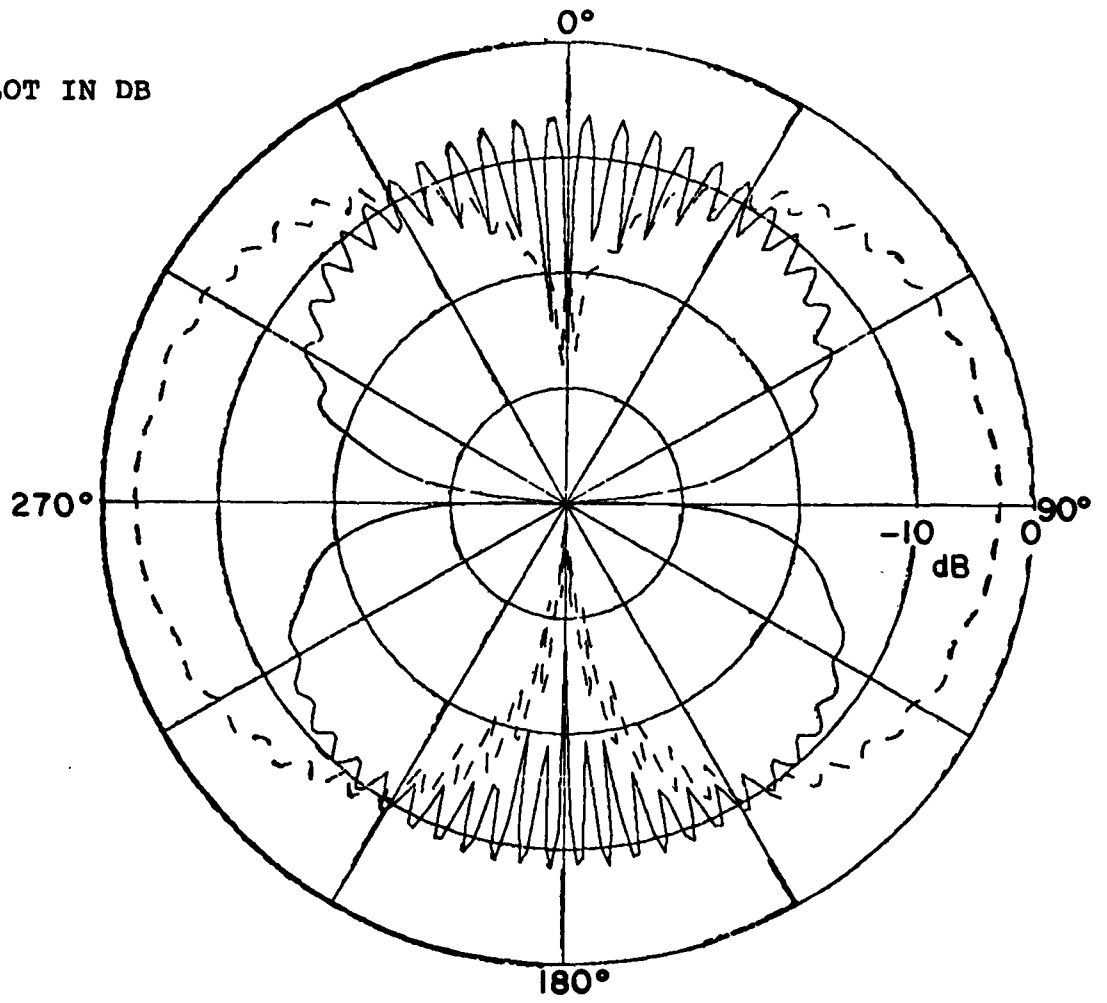

Figure 15a. Radiation patterns in azimuth plane for a short monopole mounted at ϕ_S=0°, Zs = -10 on a 4λ x 8λ x 40λ ellipsoid.

```
UN:METERS
1
FQ:0.3 GHZ
1,0.3,0.3
FG:FUSELAGE
4.,8.,40.
0.,0.,0.
SG:MONOPOLE
0.,-10.
1
0.,0.
.1,.2,0.,.01,3
1.,0.
PD:ELEVATION PLANE PATTERN (FAR FIELD)
90.,90.,130.
0,360,1
T,1000.
PP:POLAR PLOT IN DB
T
2.,2.5,3
EX:
```

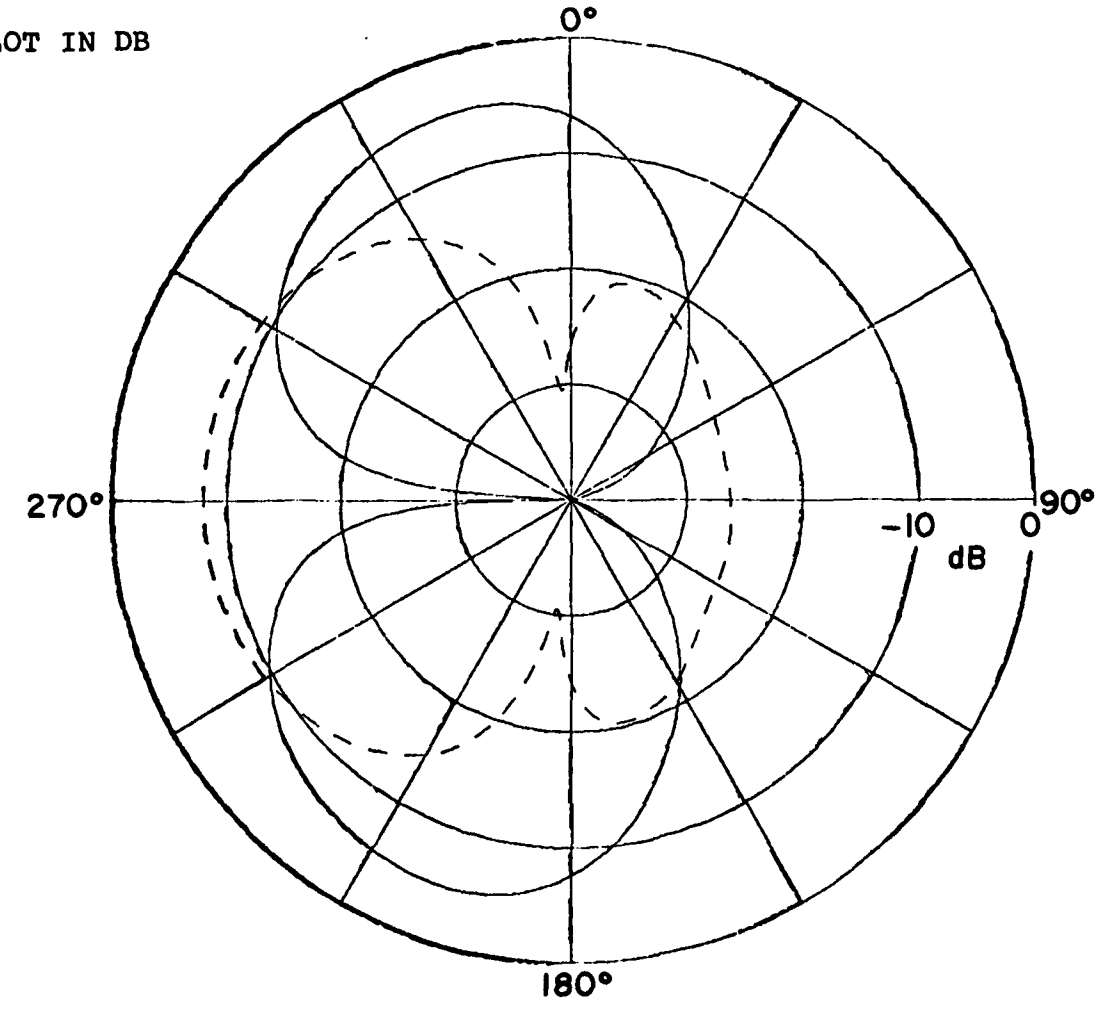

Figure 15b. Radiation patterns in elevation plane for a short monopole mounted at $\phi_S=0^\circ$, Z_S = -10 on a 4λ x 8λ x 40λ ellipsoid.

```
UN:METERS
1
FQ:0.3 GHZ
1,0.3,0.3
FG:FUSELAGE
4.,8.,40.
0.,0.,0.
SG:MONOPOLE
0.,-10.
1
0.,0.
.1,.2,0.,.01,3
1.,0.
PD:ROLL PLANE PATTERN (FAR FIELD)
0.,90.,130.
0,360,1
T,1000.
PP:POLAR PLOT IN DB
T
2.,2.5,3
EX:
```

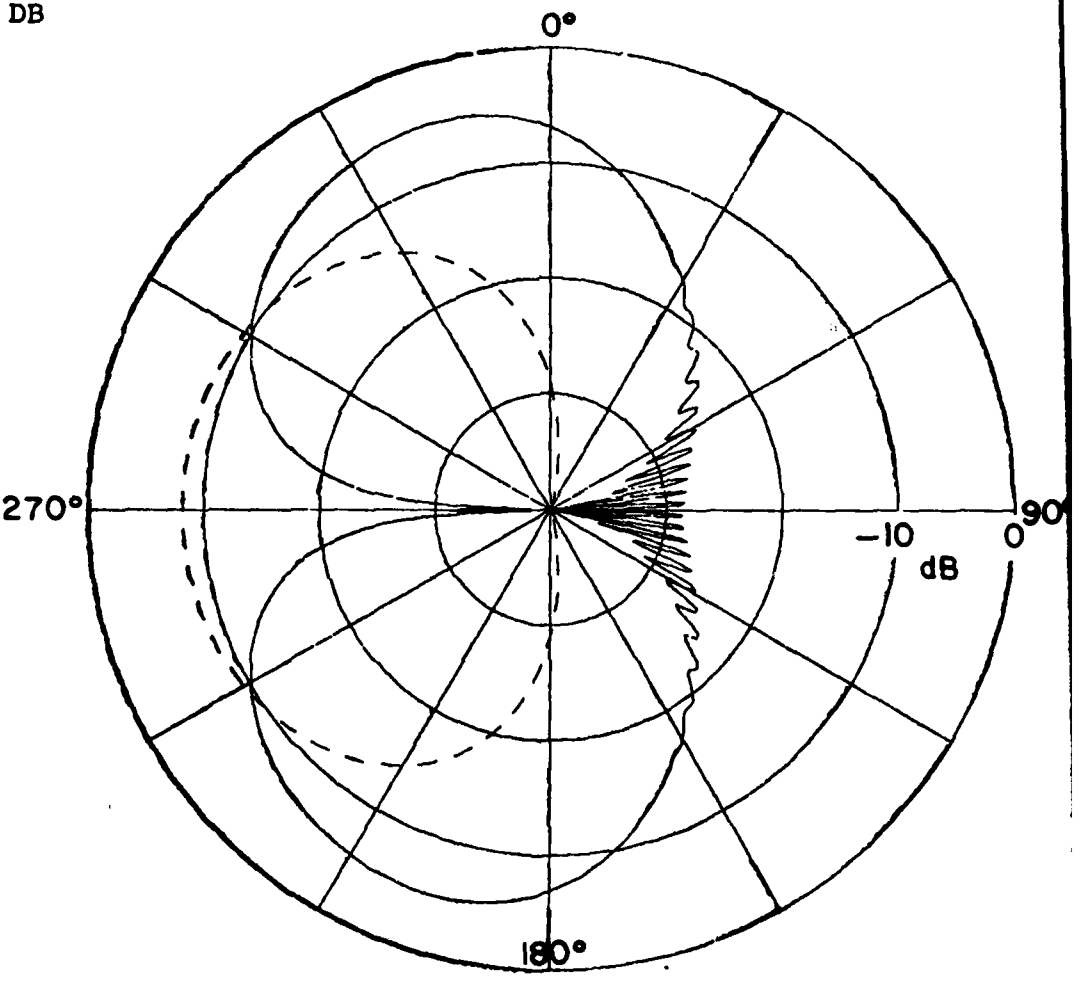

Figure 15c. Radiation patterns in roll plane for a short monopole mounted at $\phi_S=0^\circ$, Zs = -10 on a 4λ x 8λ x 40λ ellipsoid.

As a continuation of the present research effort, this geodesic solution for the ellipsoid will be employed to construct the general radiation solution along with flat plates which will be used to simulate the various appendages done earlier for the prolate spheriod model. Once this numerical solution is completed, it will be verified based on numerous comparisons with experimental results. Most of these comparisons will be in terms of actual aircraft simulations that have been used in the past for verification purposes.

The development of the ellipsoid fuselage model completes the basic research effort associated with the general topic of airborne antenna pattern analysis in terms of treating perfectly conducting structures. However, that does not imply that all the basic research problems in this general topic area have been resolved. For example, there has been a great deal of interest recently in terms of analyzing the scattering properties of dielectric structures such as an aircraft windshield, an absorber panel, or composite material. In order to treat these types of problems, a high frequency GTD solution for the scattering from finite, three-dimensional, lossless or lossy, dielectric panels has been postulated in Reference [15]. This solution needs to be added to the airborne antenna pattern analysis and verified using actual aircraft simulations. This addition to our numerical solution would provide a very significant improvement over our previous codes in that a whole new class of problems could, then, be simulated and studied.

REFERENCES

[1] W.D. Burnside, M.C. Gilreath, R.J. Marhefka and C.L. Yu, "A Study of KC-135 Aircraft Antenna Patterns," IEEE Trans. Antennas Prop., Vol. AP-23, pp. 309-316, May 1975.

[2] C.L. Yu, W.D. Burnside and M.C. Gilreath, "Volumetric Pattern Analysis of Airborne Antennas," IEEE Trans. Antennas Prop., Vol. AP-26, pp. 636-641, Sept. 1978.

[3] W.D. Burnside, N. Wang and E.L. Pelton, "Near-Field Pattern Analysis of Airborne Antennas," IEEE Trans. Antennas," IEEE Trans. Antennas Prop., Vol. AP-28, No. 3, pp. 318-327, May 1980.

[4] W.D. Burnside and N. Wang, "Research of Near Field Pattern Effects," Report 712527-4, March 1981, The Ohio State University ElectroScience Laboratory, Department of Electrical Engineering; prepared under Contract N00019-80-C-0050 for Naval Air Systems Command.

[5] C.C. Huang, N. Wang and W.D. Burnside, "The High-Frequency Radiation Patterns of a Spheroid-Mounted Antenna," Report 712527-1, March 1980, The Ohio State University ElectroScience Laboratory, Department of Electrical Engineering; prepared under Contract N00019-80-C-0050 for Naval Air Systems Command.

[6] R. Rojas-Teran and W.D. Burnside, "Curved Surface Mounted Antennas Radiating in the Presence of Perfectly Conducting Plates," Report 712527-3, July 1981, The Ohio State University ElectroScience Laboratory, Department of Electrical Engineering; prepard under Contract N00019-80-C-0050 for Naval Air Systems Command.

[7] H. Chung, W.D. Burnside and N. Wang, "The Analysis of the Curved Junction Edge Between a Flat Plate and a Prolate Spheriod," Report 713321-1, May 1981, The Ohio State University ElectroScience Laboratory, Department of Electrical Engineering; prepared under Contract N00019-80-C-0593 for Naval Air Systems Command.

[8] W.D. Burnside and H. Chung, "Simulation of Aircraft Using Prolate Spheriod Fuselage Model," Report 713321-2, to be published.

[9] P.H. Pathak, N. Wang, W.D. Burnside and R.G. Kouyoumjian, "A Uniform GTD Solution for the Radiation from Sources on a Coavex Surface," IEEE Trans. and Prop., Vol. AP-29, No. 4, July 1981.

[10] R.G. Kouyoumjian and P. Pathak, "A Uniform Geometrical Theory of Diffraction for an Edge of Perfectly Conducting Surface," Proc. IEEE, Vol. 62, pp. 1448-1461, November 1974.

[11] J.G. Kim, W.D. Burnside and N. Wang, "Geodesic Solution for an Antenna Mounted on an Ellipsoid," Report 713321-3, March 1982, The Ohio State University ElectroScience Laboratory, Department of Electrical Engineering; prepared under Contract N00019-80-PR-RJ015 for Naval Air Systems Command.

[12] J.G. Kim and W.D. Burnside, "Geodesic Paths for Side-Mounted Antenna on an Ellipsoid Model," Report 714215-1, October 1982, The Ohio State University ElectroScience Laboratory, Department of Electrical Engineering; prepared under Contract N00019-81-C-0424 for Naval Air Systems Command.

[13] J.G. Kim and W.D. Burnside, "Radiation Patterns of an Antenna Mounted on Mid-Section of Ellipsoid," Report 714215-2, to be published.

[14] J.G. Kim and W.D. Burnside, "Radiation Patterns of an Antenna Mounted on Off-Mid Section of Ellipsoid," Report 714215-3, to be published.

[15] K.M. Burgener and W.D. Burnside, "High Frequency Scattering from a Thin Lossless Dielectric Slab," Report 710964-4, November 1979, The Ohio State University ElectroScience Laboratory, Department of Electrical Engineering; prepared under Grant NSC-1498 for Langley Research Center, NASA.

END

FILMED

5-83

DTIC